The Journal of Chemical Physics

RESEARCH ARTICLE | MAY 11 2026

Comparative analysis of analytical PES-based and direct dynamics approaches in gas-phase QCT simulations of the $F^- + SiH_3I$ reaction

Attila Á. Dékány ; Balázs J. Molnár ; Gábor Czakó

J. Chem. Phys. 164, 184106 (2026)
https://doi.org/10.1063/5.0328910

The Journal of Chemical Physics ARTICLE pubs.aip.org/aip/jcp

Comparative analysis of analytical PES-based and direct dynamics approaches in gas-phase QCT simulations of the F^- + SiH_3I reaction

Cite as: J. Chem. Phys. 164, 184106 (2026); doi: 10.1063/5.0328910
Submitted: 16 February 2026 • Accepted: 20 April 2026 •
Published Online: 11 May 2026

Attila Á. Dékány, Balázs J. Molnár, and Gábor Czakó[a)]

AFFILIATIONS

MTA-SZTE Lendület "Momentum" Computational Reaction Dynamics Research Group, Interdisciplinary Excellence Centre and Department of Physical Chemistry and Materials Science, Institute of Chemistry, University of Szeged, Rerrich Béla tér 1, Szeged H-6720, Hungary

[a)]**Author to whom correspondence should be addressed:** gczako@chem.u-szeged.hu

ABSTRACT

We present a comparative analysis of analytical potential energy surface (PES)-based and direct dynamics approaches within quasi-classical trajectory simulations of gas-phase reactions. Using the analytical PES of the F^- + SiH_3I reaction as a model system, we quantify how the two methods differ in reproducing relative energies along multiple reactive pathways. High-level composite coupled-cluster energies enable a systematic decomposition of trajectory energy errors into systematic and random components over more than 8000 geometries. The analytic PES exhibits primarily random, pointwise fitting errors with mean magnitudes comparable to or smaller than the systematic deviations characteristic of lower-level electronic structure methods used in direct dynamics. A strong correlation between stationary point energy errors and trajectory-level deviations offers a practical negative indicator for assessing PES reliability. Overall, the results demonstrate that well-fitted analytical PESs can achieve accuracy equal to or greater than that of low-level direct dynamics.

I. INTRODUCTION

Theoretical chemical dynamics studies of gas-phase reactions often rely on quasi-classical trajectory (QCT)[1] simulations. These simulations can be performed using either fitted, e.g., analytical or neural-network-based, potential energy surfaces (PESs)[2–7] or the on-the-fly (direct) dynamics approach,[8] in which the forces acting on the nuclei are evaluated at each integration step through electronic structure calculations. The most challenging and time-consuming part of PES-based QCT simulations, whether using analytical or neural-network-based representations, is the development of the potential energy surface itself. The direct dynamics approach eliminates this step, allowing trajectory simulations to be run directly. However, this advantage comes at a significant computational cost. Time propagation for direct dynamics requires multiple electronic structure evaluations at every simulation step, making it several orders of magnitude more expensive than using a pre-fitted PES. Consequently, direct dynamics studies are typically limited to only a few hundred trajectories and often rely on lower-level electronic structure methods, such as Hartree–Fock (HF),[9] Møller–Plesset perturbation theory (MP2),[10] or various density functional theory (DFT) functionals,[11–15] that are faster but less accurate than high-level coupled-cluster[16] techniques. The practical reliability of these two approaches is, therefore, a critical question. Direct dynamics inherits errors from the approximation level of the underlying electronic structure theory, while analytical PESs introduce fitting errors that may vary across configuration space, even if the fitting set is obtained using arbitrarily high-quality *ab initio* methods.

Although classical and quasi-classical molecular dynamics simulations are widely used, explicit assessment of their computational quality is far less common, and it remains a nontrivial challenge to define how simulation accuracy should be evaluated in practice.[17–19] Uncertainty analysis must distinguish between systematic and random error components. Neither single trajectory behavior nor stationary-point accuracy alone is sufficient to characterize simulation reliability.[18,20–22] Robust error estimation requires large datasets covering the chemically relevant regions of the configuration space, organized into chemically meaningful groups, and compared against

high-level reference data, such as coupled-cluster energies. While several previous studies[18,20,22] have separated systematic and random errors in the context of molecular dynamics simulations, none to our knowledge has emphasized that systematic errors in the case of direct dynamics can vary significantly across configuration space. Such behavior is well known for fitted PESs but rarely examined or even expected for direct simulations.

The present study aims to compare the analytical PES-based and direct dynamics approaches by examining their ability to reproduce coupled-cluster-quality relative energies of trajectory step configurations in the model system of the gas-phase $F^- + SiH_3I$ reaction. This system provides multiple mechanistic pathways,[23] making it well suited for analyzing how different energy calculating methods behave across a diverse configuration space.

II. METHODS AND COMPUTATIONAL DETAILS

The analytical potential energy surface, PES506,[23] employed in this study was recently developed for the $F^- + SiH_3I$ system using the ROBOSURFER software,[24] which iteratively performs trajectory-guided sampling, manages *ab initio* calculations, and extends the fitting dataset until the convergence of PES fitting errors. During the development, we also monitored other PES quality indicators as well, for example, the percentage of nonphysical trajectories and root-mean-square errors between the PES and the coupled-cluster energies of the representative trajectory geometries. The PES506 is a full-dimensional permutationally invariant polynomial,[3,4] up to sixth order in Morse variables, fitted via weighted least squares to 19 492 high-level *ab initio* energy points. These energies were calculated at the ManyHF-[CCSD-F12b + BCCD(T) − BCCD]/aug-cc-pVTZ(-PP) level of theory, which is a composite coupled-cluster approach chosen for its robustness against perturbative (T) breakdown[25] and utilizing ManyHF,[26] which mitigates Hartree–Fock convergence issues.

During the development of the potential energy surface, 32 representative trajectories were used to monitor the quality of the PES.[23] These trajectories were obtained at PES376, an earlier iteration of the surface (the final version being PES506), and together provided 8371 geometries sampling the most characteristic reaction pathways. This dataset was also employed in the present comparative study. The geometries were grouped based on molecular connectivity. 3298 structures were categorized as $SiH_3I + F^-$, 1198 as $SiH_3F + I^-$, 671 as $SiH_2I^- + HF$, 525 as $SiH_2F^- + HI$, 114 as $SiHFI^- + H_2$, 255 as $SiH_2FI + H^-$, and 262 as $SiH_2 + FHI^-$. In addition, 530 structures were categorized as WMIN, 175 as FSMIN, and 169 as FSPostMIN complexes. Since WMIN and FSPostMIN share identical connectivity (see Fig. 1), we distinguished them geometrically by computing the root-mean-square deviation (RMSD) of

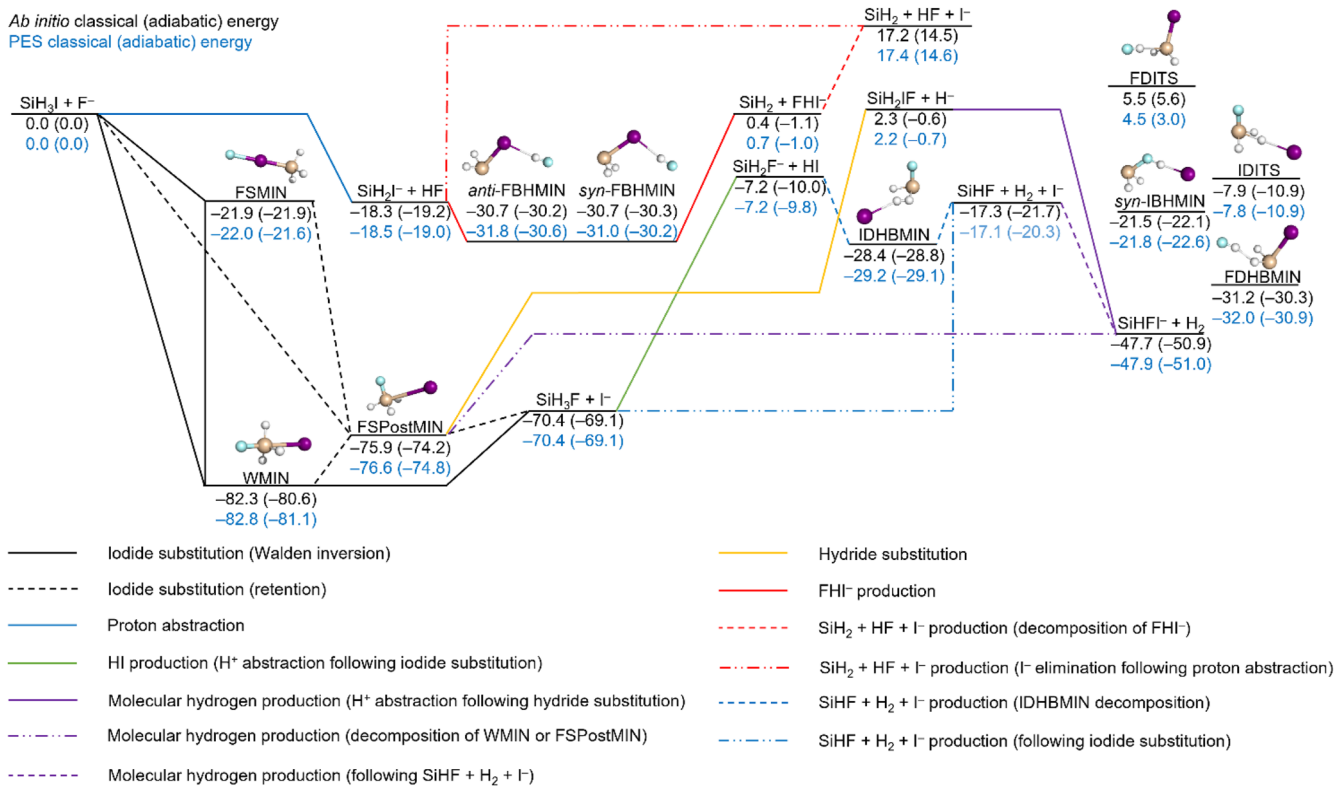

FIG. 1. Schematic PES of the $F^- + SiH_3I$ system, with structures of the stationary points and relative energies in kcal/mol. The classical *ab initio* energies are computed at the [CCSD-F12b + BCCD(T) − BCCD]/AVTZ(-PP) level of theory, and the harmonic zero-point vibrational corrections of the adiabatic energies are obtained at CCSD(T)-F12b/AVTZ(-PP).[23] Reproduced from Molnár *et al.*, J. Chem. Phys. **161**, 194306 (2024), with the permission of AIP Publishing LLC.

corresponding atoms after optimal alignment to optimized reference geometries. The remaining 1174 geometries corresponded either to strongly distorted configurations or to species represented by fewer than one hundred data points. The assignment of trajectory geometries to reference structures was performed using in-house analysis scripts based on the qcta Python package.[27,28]

All electronic structure calculations were performed using the MOLPRO program package. The coupled-cluster calculations were carried out with version 2015.1, while the rest were performed using version 2022.3.[29,30] The relative energies corresponding to each theoretical level were computed for every point in the dataset using the following methods: HF,[9] MP2,[10] B3LYP,[11,12] B3LYP-D3,[11,12,31] PBE0,[13] PBE0-D3,[13,31] M06-2X,[14] SOGGA11-X,[15] and the PES506[23] analytical potential energy surface. Thus, in addition to lower-level *ab initio* methods, we also tried several alternative DFTs, and we examined the effect of the D3 dispersion correction[31] as well. For the lighter elements (H, F, and Si), we employed the augmented correlation-consistent triple-zeta basis set, aug-cc-pVTZ.[32] For the heavier iodine atom, relativistic effects were accounted for using a relativistic effective core potential with the aug-cc-pVTZ-PP basis set.[33] We denote this basis set combination as AVTZ(-PP) throughout the article. The [CCSD-F12b + BCCD(T) − BCCD]/AVTZ(-PP) composite coupled-cluster energies ($E_{composite}$) were used as reference values (for more details see Refs. 23 and 25).

Relative energies (E_{rel}) were computed as the difference between the classical energy of each trajectory geometry and that of the $SiH_3I + F^-$ reactant optimized at the corresponding theoretical level. For the composite coupled-cluster reference, geometry optimization was performed at the CCSD(T)-F12b/AVTZ(-PP) level. For the dispersion-corrected methods, B3LYP-D3 and PBE0-D3, relative energies were evaluated using the B3LYP and PBE0 optimized structures, respectively, because test computations showed that the D3 geometry effects are negligible (<0.01 kcal/mol) on relative energies. The relative energy error for each geometry was defined as $E_{rel} - E_{rel,composite}$, where $E_{rel,composite}$ is the relative energy obtained from the composite coupled-cluster method.

For a given structural group containing N geometries, the systematic error was defined as the mean of the relative energy errors,

TABLE I. Mean relative energy errors $E_{rel} - E_{rel,composite}$ (kcal/mol) computed using various theoretical methods for geometries obtained from 32 representative trajectories (8371 geometries in total). The geometries were grouped according to molecular connectivity corresponding to stationary-point complexes, reactants, and product channels. The "other" category contains minor chemically meaningful groups with fewer than 100 structures and geometries that could not be uniquely assigned, whereas the "all" category corresponds to the entire set of geometries. All electronic structure methods were evaluated using the AVTZ(-PP) basis set. PES506[23] corresponds to the ManyHF-[CCSD-F12b + BCCD(T) − BCCD]/AVTZ(-PP) level of theory.

	HF	MP2	B3LYP	B3LYP-D3
WMIN	2.34	3.07	1.59	0.97
FSMIN	12.72	2.81	−1.05	−0.83
FSPostMIN	3.98	2.75	1.90	1.32
$SiH_3I + F^-$	1.33	0.42	−0.21	−0.22
$SiH_3F + I^-$	−6.11	3.96	0.49	0.69
$SiH_2I^- + HF$	−0.60	3.86	1.16	1.56
$SiH_2F^- + HI$	0.48	4.98	−0.87	−0.10
$SiHFI^- + H_2$	0.10	5.58	−0.18	0.06
$SiH_2FI + H^-$	−1.75	5.32	1.41	1.19
$SiH_2 + FHI^-$	−6.09	4.29	−1.44	−0.47
Other	−0.72	4.16	−0.69	−0.45
All	−0.22	2.62	0.04	0.16

	PBE0	PBE0-D3	M06-2X	SOGGA11-X	PES506
WMIN	0.34	−0.13	−1.26	2.16	−0.15
FSMIN	−2.05	−2.01	2.86	1.52	−1.20
FSPostMIN	0.24	−0.19	−0.96	2.19	−0.33
$SiH_3I + F^-$	−0.27	−0.30	0.25	0.23	−0.02
$SiH_3F + I^-$	1.64	1.68	−1.17	1.96	0.28
$SiH_2I^- + HF$	−1.50	−1.32	−2.89	1.32	0.67
$SiH_2F^- + HI$	0.05	0.46	−0.02	1.35	−0.32
$SiHFI^- + H_2$	2.22	2.32	−3.29	4.03	−0.66
$SiH_2FI + H^-$	0.93	0.79	0.47	2.19	−0.33
$SiH_2 + FHI^-$	0.26	0.78	−3.82	1.39	−0.05
Other	−0.64	−0.58	−2.62	1.88	−0.55
All	−0.03	−0.01	−0.86	1.20	−0.07

TABLE II. Standard deviation of relative energy errors $E_{rel} - E_{rel,composite}$ (kcal/mol) computed using various theoretical methods for geometries obtained from 32 representative trajectories (8371 geometries in total). The geometries were grouped according to molecular connectivity corresponding to stationary-point complexes, reactants, and product channels. The "other" category contains minor chemically meaningful groups with fewer than 100 structures and geometries that could not be uniquely assigned, whereas the "all" category corresponds to the entire set of geometries. All electronic structure methods were evaluated using the AVTZ(-PP) basis set. PES506[23] corresponds to the ManyHF-[CCSD-F12b + BCCD(T) − BCCD]/AVTZ(-PP) level of theory.

	HF	MP2	B3LYP	B3LYP-D3
WMIN	5.41	1.63	2.55	2.53
FSMIN	3.41	1.17	2.39	2.20
FSPostMIN	4.55	1.48	2.04	2.01
$SiH_3I + F^-$	1.51	0.50	0.77	0.80
$SiH_3F + I^-$	5.02	1.89	2.06	1.94
$SiH_2I^- + HF$	3.63	0.72	1.54	1.67
$SiH_2F^- + HI$	3.14	1.00	1.30	1.39
$SiHFI^- + H_2$	5.09	2.23	1.69	1.66
$SiH_2FI + H^-$	4.80	1.26	1.60	1.62
$SiH_2 + FHI^-$	3.69	0.64	1.26	1.27
Other	10.19	1.49	2.92	2.87
All	6.01	2.19	1.95	1.88

	PBE0	PBE0-D3	M06-2X	SOGGA11-X	PES506
WMIN	1.45	1.32	1.14	1.27	1.49
FSMIN	1.19	1.04	1.15	0.62	2.33
FSPostMIN	1.12	1.05	1.14	0.86	1.36
$SiH_3I + F^-$	0.54	0.56	0.58	0.46	0.69
$SiH_3F + I^-$	1.15	1.13	1.46	1.36	1.35
$SiH_2I^- + HF$	0.65	0.62	0.58	0.49	1.88
$SiH_2F^- + HI$	0.78	0.91	0.62	0.71	4.09
$SiHFI^- + H_2$	1.34	1.32	1.77	1.87	4.85
$SiH_2FI + H^-$	1.19	1.25	1.07	0.99	2.09
$SiH_2 + FHI^-$	0.93	0.96	0.47	0.42	1.38
Other	2.31	2.52	1.85	1.40	3.93
All	1.50	1.54	1.79	1.27	2.21

$$\mu = \frac{1}{N}\sum_{i=1}^{N} E_{rel,i} - E_{rel,composite,i}. \quad (1)$$

The random error was defined as the sample standard deviation of the relative energy errors,

$$\sigma = \sqrt{\frac{1}{N-1}\sum_{i=1}^{N}\left[\left(E_{rel,i} - E_{rel,composite,i}\right) - \mu\right]^2}. \quad (2)$$

Here, the mean error (μ) represents the systematic bias of a given method relative to the composite coupled-cluster reference, while the standard deviation (σ) quantifies the spread of the errors and is interpreted as a measure of the random component.

For each structural group, the mean and standard deviation of these errors were calculated and are reported in Tables I and II, enabling separate analysis of systematic and random error components. Geometries for which calculations failed to converge or produced unphysical energies ($|E_{rel} - E_{rel,composite}| > 100$ kcal/mol) were excluded. The corresponding counts are listed in Table III. Correlations between the mean relative energy errors of trajectory geometries and the relative energy errors of optimized stationary points were also examined. The relative energy errors of all optimized stationary structures are summarized in Table IV.

III. RESULTS AND DISCUSSION

A. Potential energy surface

The potential energy surface describes numerous product-forming reactions, several of which can occur via multiple mechanistic pathways, as illustrated by Fig. 1. The most significant and the most exothermic reaction of the $F^- + SiH_3I$ system is the iodide-ion substitution, leading to the formation of $SiH_3F + I^-$ with a reaction energy of $\Delta E_e(\Delta H_0) = -70.4(-69.1)$ kcal/mol. This substitution can proceed via inversion and retention mechanisms, both represented by single potential wells on the PES. The inversion pathway features a Walden-minimum (WMIN), which is also the global minimum of the surface, with a relative energy of −82.8(−81.1) kcal/mol, whereas the complex corresponding to the retention channel, FSPostMIN, lies at −76.6(−74.8) kcal/mol. Since both mechanisms are barrierless and involve the formation of deep negative-energy

TABLE III. Number of trajectory geometries omitted from the analysis due to electronic structure calculation failures (missing E_{rel} or $E_{rel,composite}$) or unphysical relative energies ($|E_{rel} - E_{rel,composite}| > 100$ kcal/mol). The counts are reported for each theoretical method and for groups of trajectory geometries classified according to molecular connectivity corresponding to stationary-point complexes, reactants, and product channels. The "other" category contains minor chemically meaningful groups with fewer than 100 structures as well as geometries that could not be uniquely assigned, whereas the "all" category corresponds to the entire dataset of 32 representative trajectories (8371 geometries). All electronic structure methods were evaluated using the AVTZ(-PP) basis set. PES506[23] corresponds to the ManyHF-[CCSD-F12b + BCCD(T) − BCCD]/AVTZ (-PP) level of theory.

	HF	MP2	B3LYP	B3LYP-D3
WMIN	0	0	0	0
FSMIN	0	0	0	0
FSPostMIN	0	0	0	0
$SiH_3I + F^-$	0	0	107	132
$SiH_3F + I^-$	0	0	6	5
$SiH_2I^- + HF$	0	0	0	0
$SiH_2F^- + HI$	0	0	6	13
$SiHFI^- + H_2$	0	0	0	0
$SiH_2FI + H^-$	2	2	35	35
$SiH_2 + FHI^-$	0	0	4	11
Other	1	1	24	31
All	3	3	182	227

	PBE0	PBE0-D3	M06-2X	SOGGA11-X	PES506
WMIN	0	0	0	0	0
FSMIN	0	0	0	0	0
FSPostMIN	0	0	0	0	0
$SiH_3I + F^-$	70	56	0	0	0
$SiH_3F + I^-$	9	8	1	4	0
$SiH_2I^- + HF$	0	0	0	0	0
$SiH_2F^- + HI$	7	6	0	3	0
$SiHFI^- + H_2$	0	0	0	0	0
$SiH_2FI + H^-$	20	21	5	8	2
$SiH_2 + FHI^-$	8	3	0	0	0
Other	33	29	2	2	1
All	147	123	8	17	3

complexes, inversion and retention iodide-ion substitutions are high probability reactions even at the lowest collision energies. Saddle points with analogous geometries to the double-inversion transition states found in previously studied carbon-centered systems also exists on the $SiH_3I + F^-$ surface, namely IDITS and FDITS. However, because the front-side attack pathway is energetically strongly favored in this silicon-centered system, the double-inversion channel remains disfavored. The front-side attack of the fluoride ion can lead to the formation of a halogen-bonded complex, FSMIN, at −22.0(−21.6) kcal/mol.

The formation of the hydride-ion substitution products, $SiH_2IF + H^-$, is slightly endothermic, with $\Delta E_e(\Delta H_0) = 2.2(-0.7)$ kcal/mol. The $SiH_2I^- + HF$ formation proton-abstraction reaction is exothermic, with $\Delta E_e(\Delta H_0) = -18.5(-19.0)$ kcal/mol, and may be followed by the formation of the FBHMIN complex, for which both *syn*- and *anti*-conformers were optimized with $\Delta E_e(\Delta H_0) = -31.0(-30.2)$ and −31.8(−30.6) kcal/mol, respectively. The decomposition of these complexes yields $SiH_2 + FHI^-$ in a nearly athermic reaction, with $\Delta E_e(\Delta H_0) = 0.7(-1.0)$ kcal/mol. The endothermic dissociation of the FHI^- leads to $SiH_2 + HF + I^-$ formation, with $\Delta E_e(\Delta H_0) = 17.4(14.6)$ kcal/mol. Among the more complex mechanisms, proton abstraction by the leaving ions following hydride- and iodide-ion substitutions is particularly significant. Following iodide substitution, the departing I^- can abstract a proton, producing $SiH_2F^- + HI$, while proton abstraction following hydride formation yields $SiHFI^- + H_2$. Both reactions are exothermic, with $\Delta E_e(\Delta H_0) = -7.2(-9.8)$ kcal/mol and $\Delta E_e(\Delta H_0) = -47.9(-51.0)$ kcal/mol, respectively. Molecular hydrogen can also form through other mechanisms; for instance, the WMIN or FSPostMIN complexes may lose H_2 in a single step if sufficient vibrational energy is available. In addition, decomposition of the dihydrogen-bonded complex (IDHBMIN), following HI production, yields $SiHF + H_2 + I^-$ with $\Delta E_e(\Delta H_0) = -17.1(-20.3)$ kcal/mol, which may be followed by recombination of SiHF and I^-. Having established the key mechanistic features of the PES, we now turn to quantifying how well various theoretical methods reproduce the associated trajectory energetics.

TABLE IV. $E_{rel} - E_{rel,composite}$ relative energy errors of stationary points (kcal/mol) computed using various theoretical methods. All electronic structure methods were evaluated using the AVTZ(-PP) basis set. PES506[23] corresponds to the ManyHF-[CCSD-F12b + BCCD(T) − BCCD]/AVTZ(-PP) level of theory.

	HF	MP2	B3LYP	B3LYP-D3
WMIN	−8.78	2.58	4.62	3.52
FSMIN	9.05	1.94	0.72	0.79
FSPostMIN	−15.17	2.76	4.26	3.15
$SiH_3I + F^-$	0.00	0.00	0.00	0.00
$SiH_3F + I^-$	−14.18	2.72	1.59	2.17
$SiH_2I^- + HF$	−2.77	3.36	2.12	2.67
$SiH_2F^- + HI$	−2.94	4.51	−0.03	0.98
$SiHFI^- + H_2$	−1.76	3.51	1.48	1.86
$SiH_2FI + H^-$	−6.27	4.72	2.91	2.65
$SiH_2 + FHI^-$	−10.42	4.06	−0.80	0.21

	PBE0	PBE0-D3	M06-2X	SOGGA11-X	PES506
WMIN	2.87	2.25	−2.90	2.92	−0.48
FSMIN	−1.79	−1.78	2.25	0.92	−0.03
FSPostMIN	3.68	3.04	−2.97	2.87	−0.70
$SiH_3I + F^-$	0.00	0.00	0.00	0.00	0.00
$SiH_3F + I^-$	2.75	3.07	−2.68	1.11	−0.01
$SiH_2I^- + HF$	−1.48	−1.16	−2.87	0.82	−0.24
$SiH_2F^- + HI$	0.45	1.01	−0.41	0.93	0.00
$SiHFI^- + H_2$	1.35	1.58	−4.88	2.38	−0.18
$SiH_2FI + H^-$	2.13	1.99	0.26	1.95	−0.03
$SiH_2 + FHI^-$	0.95	1.53	−3.87	1.30	0.36

B. Comparative analysis of QCT approaches

Figure 2 shows an iodide substitution trajectory, as an illustrative example of random and systematic relative energy errors ($E_{rel} - E_{rel,composite}$), depending on the method of energy computation and chemical configuration. Additional representative trajectory plots for all reaction channels are shown in the supplementary material (Figs. S1–S32).

The relative energies of the trajectory step geometries were obtained using PES506, and the various *ab initio* and DFT methods described above. The middle panel shows that the relative energies span a range wider than 70 kcal/mol, with high-amplitude, sudden jumps. The bottom panel, displaying the deviation from the composite coupled-cluster relative energy, provides a more informative picture of each method's accuracy. In the reactant region, the HF method exhibits a small but systematically positive bias of a few kcal/mol, while other methods show no significant systematic deviation. In the product region, however, a method-dependent systematic shift appears. In the case of HF, the relative energy errors are between −5 and −10 kcal/mol; for M06-2X, the errors are hovering around −2 kcal/mol, whereas for MP2, the errors are positive, around 2 kcal/mol. In addition to these systematic deviations, random errors are also evident, particularly for HF, which shows large rapid fluctuations. The systematic error components of other product formations differ from those of iodide substitution.

To quantify the reliability of each theoretical method, the systematic (mean) and random (standard deviation) components of the relative energy errors were analyzed. Tables I and II show that for PES506, the mean of the relative energy errors range between −1.2 and 0.7 kcal/mol, and the standard deviations of the errors are between 0.7 and 4.9 kcal/mol.

For the HF method, the mean errors span an extremely wide range, from −6.1 to 12.7 kcal/mol. In the case of MP2, all mean errors are positive, ranging from 0.4 to 5.6 kcal/mol. For the DFT methods, the range of mean errors is also a few kcal/mol wide, with B3LYP exhibiting mean errors between −1.4 and 1.9 kcal/mol, PBE0 between −2.1 and 2.2 kcal/mol, M06-2X between −3.8 and 2.9 kcal/mol, and SOGGA11-X between 0.2 and 4.0 kcal/mol. The D3 dispersion correction slightly improves the B3LYP results, with B3LYP-D3 mean errors ranging from −0.9 to 1.6 kcal/mol, and has a nearly negligible effect on PBE0, with PBE0-D3 mean errors ranging from −2.0 to 2.3 kcal/mol. Overall, PES506 achieved the smallest mean error, while none of the DFT methods reached chemical accuracy (absolute mean errors below 1 kcal/mol). The MP2 method showed consistent positive bias, and HF exhibited unacceptably high deviations.

High standard deviations in relative energies imply that geometries differing only slightly may carry significantly different errors. Since numerical gradient calculations, used by many trajectory propagation algorithms, are sensitive to such fluctuations, assessing the standard deviation of relative energy errors along the trajectory is also necessary. For the Hartree–Fock method, all standard deviations exceed 1 kcal/mol, ranging from 1.5 to 5.4 kcal/mol. For the MP2 and DFT methods, standard deviations span from 0.4 kcal/mol at the lowest to 2.6 kcal/mol at the highest. The D3 dispersion

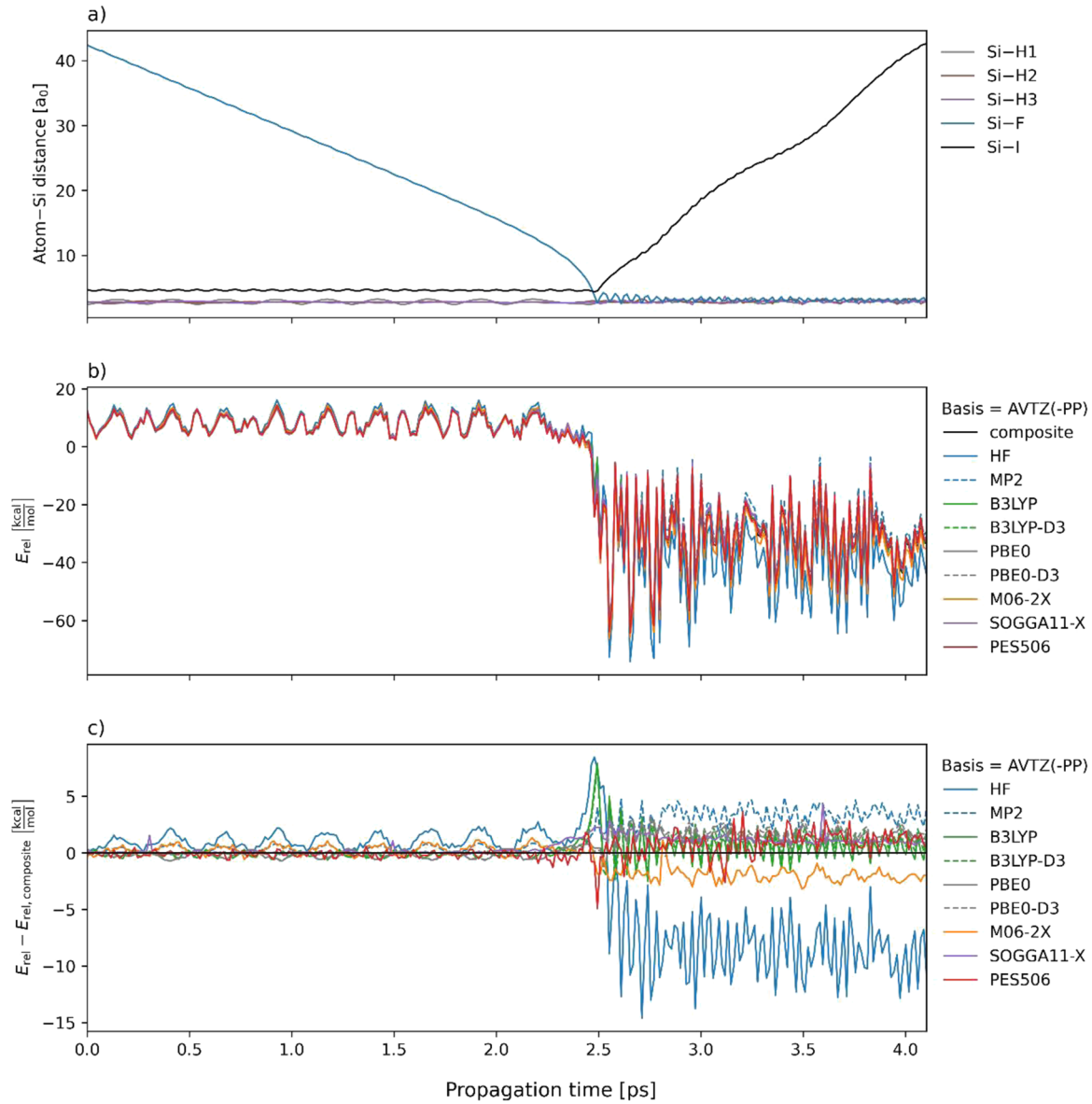

FIG. 2. A representative iodide-ion substitution trajectory. The upper panel (a) shows the time evolution of the atom–central atom distances, the middle panel (b) shows the relative energies obtained at different theoretical levels, and the lower panel (c) displays the corresponding relative energy errors. The relative energy error is defined as the difference between the value calculated at a given theoretical level and the reference relative energy obtained at [CCSD-F12b + BCCD(T) − BCCD]/AVTZ(-PP). All energies are relative to the classical energy of the reactant structure optimized at their corresponding theoretical level. The optimized reference reactant geometry is of CCSD(T)-F12b/AVTZ(-PP) quality.

correction does not significantly reduce the random error component for either B3LYP or PBE0. For PES506, the standard deviations of the relative energy errors range from 0.7 to 4.9 kcal/mol, meaning that most product channels are described with a moderate random error component comparable to the noise level of the DFT methods, whereas a few lower-probability reactions, such as HI and H_2 formation, exhibit larger random errors.

Figure 3 was constructed using the data from Tables I, II, and IV. The figure shows the correlation between the mean relative energy errors of the trajectory geometries and the errors in the relative energies of the stationary points optimized at various theoretical levels. The vertical error bars represent the standard deviations of the relative energy errors. Supporting this statistical representation, the distributions of the relative energy errors for all structural groups are

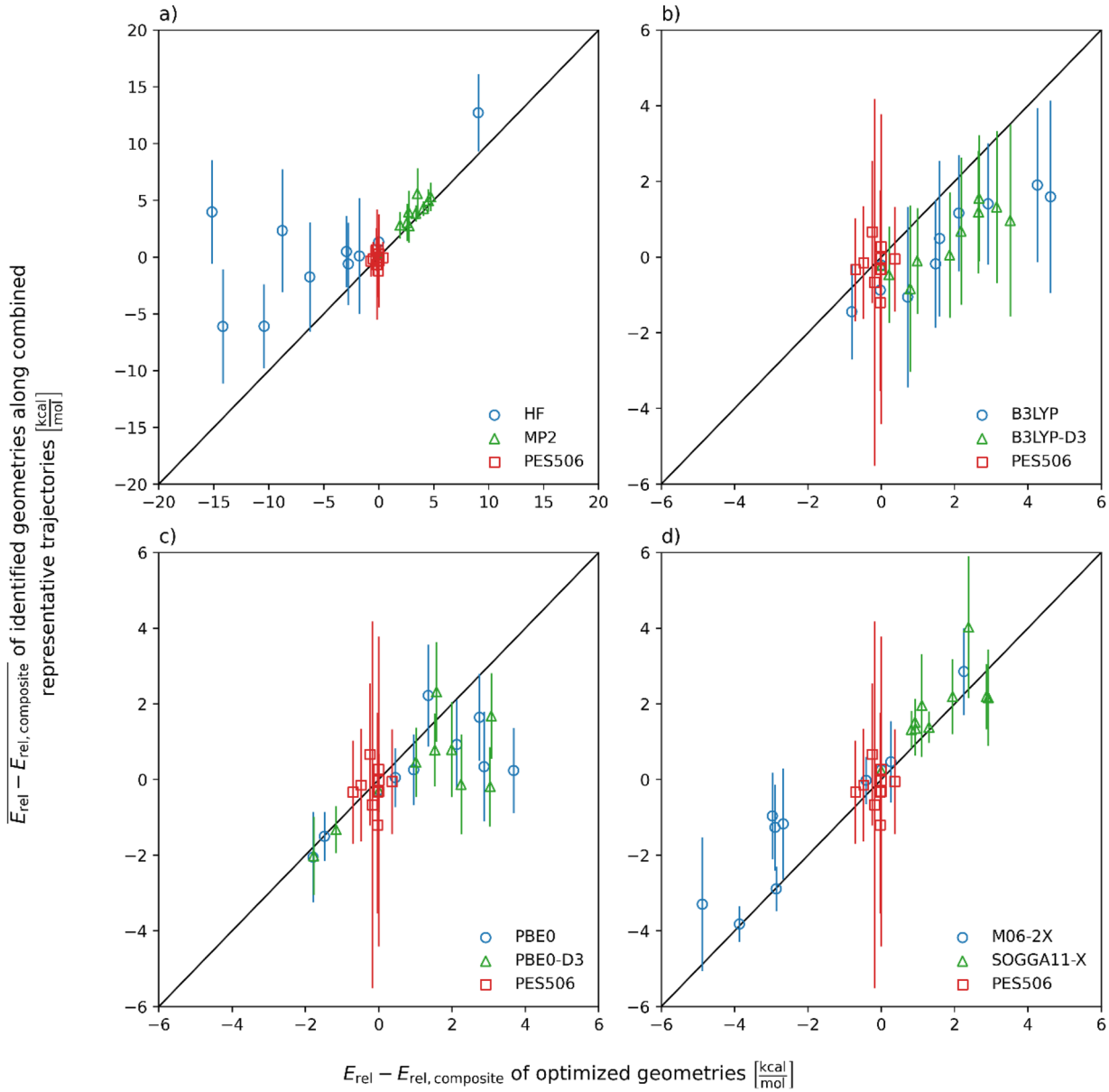

FIG. 3. Correlation between the mean relative energy errors of trajectory geometries mapped to stationary points and the deviations of the corresponding optimized stationary-point energies from the composite ([CCSD-F12b + BCCD(T) − BCCD]/AVTZ(-PP)) reference. The vertical error bars represent the standard deviations of the trajectory data. The black diagonal line indicates perfect correlation. The optimized reference geometries are of CCSD(T)-F12b/AVTZ(-PP) quality. Panel (a) shows HF, MP2, and PES506 results; panel (b) shows B3LYP, B3LYP-D3, and PES506; panel (c) shows PBE0, PBE0-D3, and PES506; and panel (d) shows M06-2X, SOGGA11-X, and PES506. The same PES506 data points are repeated in all panels for consistent visual comparison.

shown in the supplementary material (Figs. S33–S36). These distributions closely approximate bell-shaped profiles, indicating that the deviations can be characterized by their mean and standard deviation. For the MP2, M06-2X, and SOGGA11-X methods, a clear correlation is observed as most data points intersect the black line representing perfect correlation within their standard deviation. For the B3LYP and PBE0 methods, this correlation is less apparent, as a significant fraction of the points falls below the correlation line in the region of positive $E_{rel} - E_{rel,composite}$ values. This indicates that B3LYP and PBE0 reproduce product channels with positive relative energy errors with smaller-than-expected deviations. For the HF method, the points are too widely scattered for any correlation to be detected. The PES506 data points stand out clearly from the rest, clustering around zero, which reflects the characteristically low

systematic error of the analytical PES-based approach. Based on the standard deviations, the random error of trajectories propagated on the analytical PES is in several cases larger than that of MP2 and the DFT methods, whereas for product channels well described by the PES, the scatter is comparable to that of the methods typically used in direct dynamics. Our overall conclusion is that, based on the random component of the relative energy errors, the analytical PES method exhibits reliability comparable to or better than direct dynamics for mechanisms well represented in the fitting set, and based on the systematic error contribution, the fitted PES is generally more reliable. This latter observation is supported by the correlation between the errors in the relative energies of stationary points optimized at lower levels of theory and the mean relative energy errors of the corresponding trajectory structures. The relative energies of stationary points optimized on PESs fitted to high-quality datasets generally deviate only slightly, within 1 kcal/mol, from the direct *ab initio* values.

Table III showing the discarded geometries also provides additional insight into the applicability and limitations of direct dynamics. For the B3LYP, B3LYP-D3, PBE0, and PBE0-D3 methods, 182, 227, 147, and 123 geometries, respectively, could not be included in the analysis because the energy calculations failed (either the DFT or the coupled-cluster reference calculation did not converge, or unphysical energies were obtained). These correspond to 2.1%, 2.7%, 1.8%, and 1.5% of the total dataset. Such failure rates suggest that a simple implementation of direct dynamics using these methods may frequently terminate due to electronic structure calculation errors. The discarded geometries are not distributed uniformly across the dataset but are more common for certain reaction pathways. For example, among the low-probability reactions, 14% of the hydride-substitution products (structures of $SiH_2FI + H^-$) fall into the discarded category for B3LYP and B3LYP-D3, and nearly 8% for PBE0 and PBE0-D3. For the other two DFT methods, the number of discarded geometries is substantially smaller. In the case of M06-2X and SOGGA11-X, only 8 and 17 geometries were excluded, respectively (~0.1% and 0.2% of the total dataset). A significant fraction of these geometries also corresponds to hydride substitution products. For the Hartree–Fock, MP2, and PES506 methods, three geometries lack relative energy errors. However, this is not due to failures of these methods. It results from three unsuccessful coupled-cluster reference calculations, which prevent the evaluation of $E_{rel} - E_{rel,composite}$ for those geometries.

To assess whether the selective exclusion of these geometries could bias the statistical analysis, the correlation analysis shown in Fig. 3 was repeated using the smallest common subset of geometries available for all methods. This was achieved by removing additional geometries from the $SiH_3I + F^-$, $SiH_3F + I^-$, $SiH_2F^- + HI$, $SiH_2FI + H^-$, $SiH_2 + FHI^-$, and "other" groups, yielding a common dataset of exactly 8000 geometries. The resulting correlations were essentially unchanged (see Fig. S37), indicating that the omission of the discarded points does not significantly affect the statistical conclusions. Using identical subsets for all methods would, therefore, not alter the interpretation of the results, and the full dataset was retained for the primary analysis.

Finally, it is worth noting that both direct dynamics and fitted PES-based approaches can discover new reaction pathways. For fitted PESs, this capability may appear less obvious, because the early stages of their construction usually rely primarily on known stationary points and a limited region of configuration space. However, during the iterative development process, the trajectories progressively explore new regions of configuration space. Numerous unexpected mechanisms have been identified using fitted PESs. For example, the double-inversion S_N2 mechanism in carbon-centered systems was discovered using an analytical potential energy surface.[34] In addition, in our earlier study of the $SiH_3Cl + F^-$ system, the HCl and H_2 formation reactions emerged during the PES development process without prior knowledge of their existence.[35] Based on our experience, qualitatively new mechanisms can already appear even on moderately developed fitted PESs with relatively large fitting errors. In the final stage of development, the trajectory-level relative energy errors decrease, while measurable properties, such as cross sections, converge across successive PES iterations.

IV. SUMMARY AND CONCLUSIONS

This study presents a comparative analysis of analytical PES-based and direct dynamics approaches within the framework of QCT simulations for gas-phase reactions. While direct dynamics eliminates the need to construct an analytical PES by evaluating electronic energies at each integration step, it remains computationally demanding, and in practice, it often relies on lower-level electronic structure methods. In contrast, analytical PES-based dynamics is orders of magnitude more efficient but introduces fitting-related errors that depend on the fitting strategy and on the quality, coverage, and representativeness of the underlying *ab initio* dataset. Using the $F^- + SiH_3I$ gas-phase reaction as a model system, this study systematically examines how analytical PES-based and direct dynamics approaches differ in their ability to reproduce relative energies along reactive trajectories. High-level composite coupled-cluster energies serve as the reference, allowing a detailed assessment of errors across a recently developed analytical potential energy surface (PES506)[23] and multiple electronic structure methods, including HF, MP2, and several DFT functionals. A central contribution of the present work is the quantitative decomposition of trajectory energy errors into systematic and random components, evaluated over more than 8000 trajectory geometries. These geometries sample the most characteristic regions of the model PES, including high-probability reactions, such as iodide-ion substitution and proton abstraction, and lower-probability channels leading to HF, HI, H_2, H^-, and FHI^- formations. The analysis shows that the coupled-cluster quality analytical PES primarily exhibits random, pointwise fitting errors whose average magnitudes are comparable to, or smaller than, the systematic deviations characteristic of lower-level electronic-structure methods typically employed in direct dynamics simulations. Furthermore, a clear correlation is observed between the energy errors of optimized stationary points and the mean trajectory-level deviations for the present system, suggesting that stationary-point energetics may serve as a useful indicator of PES quality. Large errors in stationary-point energetics can act as a practical negative indicator, signaling that the corresponding dynamical simulations are likely to be unreliable. We should note that the opposite is not generally true. Chemically accurate stationary-point energetics does not guarantee accurate dynamics, as reaction outcomes are also

governed by the global shape of the PES, including non-stationary regions.[21] Overall, the analytical PES-based approach demonstrates equal or superior reliability compared to low theoretical level direct dynamics for mechanisms well represented by the fitted data. This study, thus, challenges the assumption that direct *ab initio* dynamics is inherently more accurate, highlighting that analytical PES methods, when properly developed, can achieve comparable or better fidelity at far lower computational cost. By introducing a framework for separating and quantifying systematic and random errors in trajectory energetics, this work extends uncertainty quantification concepts into QCT methodology and provides a new perspective for evaluating the practical reliability of classical and quasi-classical molecular dynamics simulations.

SUPPLEMENTARY MATERIAL

The supplementary material provides representative trajectory plots for all major and minor reaction channels of the F^- + SiH_3I system, showing atom–central atom distances, relative energies computed at different theoretical levels, and the corresponding relative energy errors with respect to the composite coupled-cluster reference (Figs. S1–S32). In addition, the detailed distributions of relative energy errors are also provided (Figs. S33–S36) as well as correlation between the mean relative energy errors of trajectory geometries mapped to stationary points and the deviations of the corresponding optimized stationary-point energies from the composite reference, computed using the smallest common dataset available for all methods (Fig. S37).

ACKNOWLEDGMENTS

We thank the National Research, Development and Innovation Office–NKFIH, Grant No. K-146759, and the Momentum (Lendület) Program of the Hungarian Academy of Sciences for financial support.

AUTHOR DECLARATIONS

Conflict of Interest

The authors have no conflicts to disclose.

Author Contributions

Attila Á. Dékány: Conceptualization (equal); Data curation (supporting); Formal analysis (lead); Investigation (equal); Software (lead); Visualization (lead); Writing – original draft (lead); Writing – review & editing (equal). **Balázs J. Molnár**: Data curation (lead); Formal analysis (supporting); Investigation (equal); Visualization (supporting); Writing – original draft (supporting); Writing – review & editing (supporting). **Gábor Czakó**: Conceptualization (equal); Funding acquisition (lead); Project administration (lead); Supervision (lead); Writing – original draft (supporting); Writing – review & editing (equal).

DATA AVAILABILITY

The data that support the findings of this study are available in Tables I–IV and from the corresponding author upon reasonable request.

REFERENCES

[1] W. L. Hase, *Encyclopedia of Computational Chemistry* (Wiley, New York, 1998), pp. 399–407.
[2] R. Dawes, D. L. Thompson, Y. Guo, A. F. Wagner, and M. Minkoff, J. Chem. Phys. **126**, 184108 (2007).
[3] B. J. Braams and J. M. Bowman, Int. Rev. Phys. Chem. **28**, 577 (2009).
[4] J. M. Bowman, G. Czakó, and B. Fu, Phys. Chem. Chem. Phys. **13**, 8094 (2011).
[5] B. Jiang, J. Li, and H. Guo, J. Phys. Chem. Lett. **11**, 5120 (2020).
[6] Y. Liu and H. Guo, J. Phys. Chem. A **127**, 8765 (2023).
[7] B. Fu and D. H. Zhang, Natl. Sci. Rev. **10**, nwad321 (2023).
[8] M. Paranjothy, R. Sun, Y. Zhuang, and W. L. Hase, WIREs Comput. Mol. Sci. **3**, 296 (2013).
[9] W. J. Hehre, L. Radom, P. v. R. Schleyer, and J. A. Pople, *Molecular Orbital Theory* (Wiley, New York, 1986).
[10] C. Møller and M. S. Plesset, Phys. Rev. **46**, 618 (1934).
[11] A. D. Becke, J. Chem. Phys. **98**, 5648 (1993).
[12] C. Lee, W. Yang, and R. G. Parr, Phys. Rev. B **37**, 785 (1988).
[13] C. Adamo and V. Barone, J. Chem. Phys. **110**, 6158 (1999).
[14] Y. Zhao and D. G. Truhlar, Theor. Chem. Acc. **120**, 215 (2008).
[15] R. Peverati and D. G. Truhlar, J. Chem. Phys. **135**, 191102 (2011).
[16] T. B. Adler, G. Knizia, and H.-J. Werner, J. Chem. Phys. **127**, 221106 (2007).
[17] A. Grossfield, P. N. Patrone, D. R. Roe, A. J. Schultz, D. W. Siderius, and D. M. Zuckerman, Living J. Comput. Mol. Sci. **1**, 5067 (2019).
[18] S. Wan, R. C. Sinclair, and P. V. Coveney, Philos. Trans. R. Soc. A **379**, 20200082 (2021).
[19] G. Imbalzano, Y. Zhuang, V. Kapil, K. Rossi, E. A. Engel, F. Grasselli, and M. Ceriotti, J. Chem. Phys. **154**, 074102 (2021).
[20] A. V. Tran and Y. Wang, Comput. Mater. Sci. **127**, 141 (2017).
[21] T. Győri, B. Olasz, G. Paragi, and G. Czakó, J. Phys. Chem. A **122**, 3353 (2018).
[22] S. Goswami, S. Käser, R. J. Bemish, and M. Meuwly, Artif. Intell. Chem. **2**, 100033 (2024).
[23] B. J. Molnár, A. Á. Dékány, and G. Czakó, J. Chem. Phys. **161**, 194306 (2024).
[24] T. Győri and G. Czakó, J. Chem. Theory Comput. **16**, 51 (2020).
[25] D. A. Tasi, T. Győri, and G. Czakó, Phys. Chem. Chem. Phys. **22**, 3775 (2020).
[26] T. Győri and G. Czakó, J. Chem. Phys. **156**, 071101 (2022).
[27] See https://gitlab.com/d_attila/qcta for the source code of the qcta (quasi-classical trajectory analyser) Python package.
[28] See https://d_attila.gitlab.io/qcta/index.html for the online documentation of qcta.
[29] H.-J. Werner, P. J. Knowles, G. Knizia, F. R. Manby, M. Schütz *et al.*, MOLPRO, version 2015.1, a package of *ab initio* programs, see http://www.molpro.net.
[30] H.-J. Werner, P. J. Knowles *et al.*, MOLPRO, version 2022.3, a package of *ab initio* programs, see https://www.molpro.net.
[31] S. Grimme, J. Antony, S. Ehrlich, and H. Krieg, J. Chem. Phys. **132**, 154104 (2010).
[32] T. H. Dunning, Jr., J. Chem. Phys. **90**, 1007 (1989).
[33] K. A. Peterson, D. Figgen, E. Goll, H. Stoll, and M. Dolg, J. Chem. Phys. **119**, 11113 (2003).
[34] I. Szabó and G. Czakó, Nat. Commun. **6**, 5972 (2015).
[35] A. Á. Dékány and G. Czakó, J. Chem. Phys. **158**, 224303 (2023).